Available online at www.sciencedirect.com
SCIENCE DIRECT®
Coordination Chemistry Reviews 248 (2004) 2409–2424
COORDINATION CHEMISTRY REVIEWS
www.elsevier.com/locate/ccr

Review

In situ mechanistic studies in rhodium catalyzed hydroformylation of alkenes

Paul C.J. Kamer*, Annemiek van Rooy, Gerard C. Schoemaker, Piet W.N.M. van Leeuwen

Van't Hoff Institute for Molecular Sciences, University of Amsterdam, Nieuwe Achtergracht 166, 1018 WV Amsterdam, The Netherlands

Received 17 June 2004; accepted 18 June 2004
Available online 14 August 2004

Contents

Abstract

A new in situ high-pressure IR (HP-IR) autoclave is presented that is especially suited for mechanistic studies of fast catalytic reactions. This review summarizes several applications of the HP-IR cell in the rhodium catalyzed hydroformylation of alkenes. The most abundant species during the very fast hydroformylation of 1-alkenes using tris(2-*tert*-butyl-4-methylphenyl) phosphite was identified as the Rh acyl complex $RhC(O)R(CO)_3L$. A detailed kinetic study and (in situ) spectroscopic techniques revealed that when a monodentate biuret-based phosphorus diamide ligand is used several of the elementary reaction steps are involved in the hydroformylation rate control. Depending on the reaction conditions, the rate-determining step is early or late in the catalytic cycle. The rates of single steps of the catalytic hydroformylation cycle could be determined using labeling experiments. The use of ^{13}CO labeling in rapid-scan IR experiments to determine the rate of CO dissociation in the (diphosphine)$Rh(CO)_2H$ complexes is described. Furthermore, the H/D exchange rate of $DRh(L–L)(CO)_2$ with H_2 was measured using rapid-scan high-pressure IR spectroscopy. Finally, the HP IR cell was used to identify the reaction between the most likely impurities in alkene feeds and the rhodium catalyst.

Keywords: Hydroformylation; Ligands; NMR

1. Introduction

To date the hydroformylation reaction is one of the most important homogeneously catalyzed reactions in the world, covering an annual production of almost eight million tons of aldehydes and alcohols [1]. Consequently, hydroformylation

* Corresponding author. Tel.: +31 20 525 6495; fax: +31 20 525 5604.
E-mail address: kamer@science.uva.nl (P.C.J. Kamer).

0010-8545/$ – see front matter © 2004 Elsevier B.V. All rights reserved.
doi:10.1016/j.ccr.2004.06.006

is one of the most extensively studied homogeneous catalytic processes. Improvement of rates and selectivities by ligand design as well as mechanistic aspects receive much attention. The large impact of phosphine ligands became evident by the important discovery of the Wilkinson hydrogenation catalyst, $RhCl(PPh_3)_3$ [2]. Substitution at the aromatic ring of the ligand revealed an electronic effect on the reaction rate, illustrating the distinct ligand effect on the reactivity of a transition metal complex. Ever since, an impressive number of phosphine ligands have been applied in many catalytic reactions and it became obvious that the steric and electronic properties of the ligands have an enormous effect on the reactivity of metal complexes. The huge effects that were observed called for a systematic classification of ligand properties.

Strohmeier showed that the IR carbonyl frequencies of metal complexes could be used as a measure of the electronic properties of ligands [3]. Tolman introduced a systematic approach to describe steric and electronic ligand effects [4]. For phosphorus ligands the cone angle θ (Fig. 1) is defined as the apex angle of a cylindrical cone, centered at 2.28 Å from the center of the P atom, which touches the outermost atoms of the model. The electronic parameter χ is based on the difference in the IR frequencies of $Ni(CO)_3L$ and the reference compound $Ni(CO)_3$(P-*tert*-Bu_3).

The concepts of the *natural bite angle* and the *flexibility range* for diphosphine ligands are a means to predict chelational preferences of bidentate ligands [5]. The natural bite angle (β_n) is defined as the preferred chelation angle determined by ligand backbone only and not by metal valence angles. The flexibility range is defined as the accessible range of bite angles that induce less than 3 kcal mol^{-1} excess strain energy compared to the calculated natural bite angle.

The development of organotransition metal chemistry has largely contributed to the enormous growth of homogeneous catalysis [6]. Knowledge about bonding and reactivity in organometallic chemistry has been of great support to catalysis [7]. The reactivity of organotransition metal complexes is dependent on the ligand environment of the metal. By changing the ligands the performance of the catalyst can be directed and sometimes the effects can even be predicted. In transition metal catalysis extensive research has been devoted to fine-tune the selectivity and activity of catalysts by means of ligand modification, just simply by looking at electronic and steric effects. In this way many processes have been improved and several new ones have been developed. In depth understanding of a catalytic reaction, however, requires mechanistic studies under actual catalytic conditions. Characterization of reaction intermediates during the rhodium catalyzed hydroformylation has only scarcely been performed. This is probably due to the difficulties arising when spectroscopic studies need to be carried out under high pressure and temperature, like mass transfer limitations in combination with low concentrations of the catalytically active metal complex.

Today, high pressure NMR is a regularly applied technique for the identification of organometallic compounds under high pressure [8]. To obtain satisfactory signal to noise

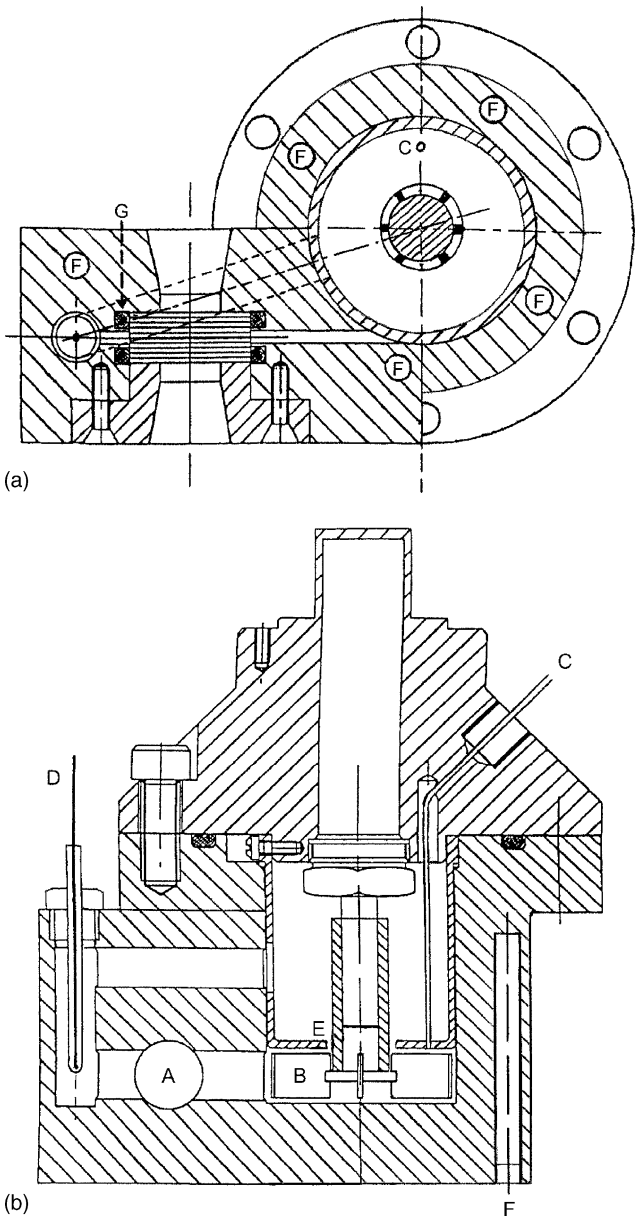

Fig. 1. Side- and top-view of the in situ infrared autoclave: (A) IR windows; (B) turbine rotor; (C) reagent addition; (D) thermocouple; (E) opening between upper and lower chamber; (F) electrical heaters; (G) Kalrez® O-rings.

ratios high concentrations in a small reaction vessel are required. As a result the gas volume above the solution is often too small to allow us to follow a fast catalytic reaction for a longer time. To avoid mass-transfer limitations special flow cells are required, as developed by Iggo et al. [9], but still higher than "catalytic" concentrations are required. Infrared spectroscopy offers in this respect better perspectives regarding sensitivity [10]. Very often the catalytic species is a transition metal carbonyl complex of which the CO vibrations have strong absorptions. Hence, low concentrations that approach actual catalysis conditions in hydroformylation chemistry are realizable. Already in the sixties Noack described a high-pressure autoclave for infrared measurements [11]. The

catalytic reaction was carried out in an external high-pressure autoclave, with a magnetically actuated piston and a non-return valve for both mixing and continuously pumping the reactor batch through a high-pressure transmission cell. King et al. used a reactor assembled directly on top of the infrared cell where an electronically timed mechanical agitator forced the solvent through the infrared windows [12]. Moser et al. embedded a cylindrical internal reflection crystal (CIR) into a standard Parr Mini Reactor [13]. This is an elegant set-up for real in situ measurements but disadvantages of that system are the relatively low signal-to-noise ratios, the temperature and frequency dependence of the penetration depth in solution, and restrictions in solvent use by the employment of a selected CIR crystal.

As early as 1968 Wilkinson performed a study of the PPh3 modified rhodium hydroformylation catalyst in situ [14]. Although the reaction conditions in the IR cell, connected via a tube with the autoclave, probably were already suffering from mass transfer limitations, he characterized several intermediate complexes that are only stable under CO pressure, such as $HRhP_2(CO)_2$ (with P = phosphine). Furthermore, he was the first who listed infrared data of some rhodium alkyl and rhodium acyl complexes. A comparable study was performed more recently by Moser et al. [13] who applied their cylindrical internal reflectance IR cell. He studied the triphenylphosphine modified rhodium catalyst in the presence of substrate in order to determine the rate-limiting step of the reaction. He varied the electron-accepting properties of the ligand by substituting the phenyl rings of the PPh_3 and found that the rates of the different reaction steps had changed. He also identified some inactive rhodium dimers as a result of decomposition of the active hydrido species. However, the used CIR technique shows a rather low signal to noise ratio and long measuring times are necessary and therefore, it cannot be applied in very fast reacting systems. A very extensive and careful study was carried out by Garland on phosphine-free systems [15]. Under very high pressures he was able to identify the very unstable complex $RhR(CO)_4$ (with R = neohexyl) and additionally $RhRC(O)(CO)_4$. He even performed a kinetic study in the IR autoclave.

Earlier, we presented a kinetic study of the bulky phosphite modified rhodium catalyzed hydroformylation of oct-1-ene, styrene and cyclohexene [16]. With a rate of 40,000 mol [mol Rh]$^{-1}$ h^{-1} (P = 20 bar H_2/CO, T = 80 °C, 0.002 mmol Rh, 0.1 mmol tris(2-*tert*-butyl-4-methyl)phenyl phosphite, 20 mmol oct-1-ene in 20 mL of toluene) this is an extremely fast reaction. We found for the oct-1-ene and styrene substrates a kinetic expression different from the usual ligand modified hydroformylation reactions. For cyclohexene, in accordance with expectations, a first order dependency on the substrate concentration was found. Here, the $HRhP(CO)_3$ complex is the major species during the catalysis, as was shown before by Jongsma et al. [17]. The hydroformylation of oct-1-ene and styrene showed no dependency on the substrate concentration up to a high conversion. The simultaneously observed first order in H_2 and minus first order in CO indicated that the last step in the reaction cycle, the hydrogenolysis of the acyl rhodium complex, was rate determining. This suggested that a species different from the hydrido complex is predominantly present during the catalysis. The study of such a fast reaction required the development of a new in situ IR autoclave with a higher sensitivity than the CIR cell but a reduced residence time of the sample outside the reactor.

2. In situ IR autoclave

The autoclave (see Fig. 1) consists of a stainless steel beaker that is closed with a flange cover. Some of its specifications are summarized in Table 1 [18]. The cover is provided with an electromagnetically driven mechanical stirrer of which the rotation speed can be controlled by applying an optical tachometer. The beaker consists of an upper and a lower compartment. The six-blades turbine rotor is located in the small lower compartment. The rotor blades force the solution from the bottom of the vessel through the infrared windows and loop wise back into the beaker. The solution flows back via the upper chamber around the axis of the rotor into the mixing chamber, maintaining a continuous flow in the reactor.

The whole system (including the infrared windows) can be brought under pressure and heated by means of electrical heaters. The autoclave is equipped with a temperature controller and a pressure device. Liquid or dissolved reagents (up to 1 mL) can be added, by means of a separately pressurized reservoir, directly in the lower chamber to achieve rapid mixing. The autoclave can be tightened to its position in the spectrometer by two adjustable rubber covered metal rings that simultaneously seclude moisture from the optical bench by flushing with dried air. The total volume of the autoclave is 50 ml.

The windows are made of ZnS, each 4.5 mm thick and having a diameter of 20 mm, with an optical diameter of 10 mm. The cylindrical surfaces of the windows were highly polished providing a good seal with the enclosed Kalrez O-rings. The

Table 1
Some specifications of the high-pressure in situ autoclave

Total volume (mL)	50
Volume of circulated liquid in side-loop (mL)	0.35
Maximum stirring speed (rpm)	3400
Circulation velocity at maximum speed (mL s^{-1})	4–12
Infrared windows	ZnS, transparant up to 700 cm^{-1}, ϕ 10 mm
Optical path length (mm)	0.4
Maximum pressure, temperature	185 bar at T = 200 °C
Closures	The cover of the autoclave is secured by a Viton® O-ring, the IR windows by Kalrez® O-rings

edges were round shaped to prevent damaging the O-rings during mounting. For different optical path lengths the spacing can be varied easily by changing the teflon spacer between the window and the flange with another of different thickness. The maximum pressure of the autoclave is set up to 185 bar at $T = 200\,^{\circ}C$.

The loop wise circulation velocity of the solution in the autoclave was measured by collecting the flow after the infrared windows into a measuring cylinder at different rotation velocities. Using an optical path length of 0.4 mm we observed a flow rate of 1.4–7.7 ml s^{-1} with circulation velocities between 1000 and 2500 rpm. Different optical path lengths showed a proportional change in circulation velocities. Most of the catalytic experiments were performed using 15 ml of solvent, 0.4 mm optical path length and 2200 rpm circulation speed.

The volume between the exit of the autoclave beaker and the center of the infrared windows is 0.35 ml. At 0.4 mm optical path length and 2200 rpm circulation velocity the reaction mixture reaches the center of the infrared beam after 56 ms. This time delay can be reduced to 33 ms at maximum stirring rate. To ensure efficient mixing between the upper and lower chambers the total volume is kept low.

3. Rhodium catalyzed hydroformylation

3.1. In situ IR study of rhodium bulky phosphite catalyzed hydroformylation

On addition of tris(2-*tert*-butyl-4-methylphenyl)phosphite to the rhodium precursor, immediately a spectrum is observed where the two CO stretch vibrations of $Rh(CO)_2Acac$ (2080, 2012 cm^{-1}) are replaced by one vibration at 2015 cm^{-1}, in accordance with substitution of one CO by a phosphite, resulting in formation of RhAcac(CO)P (P = phosphite). Pressurizing the HP-IR cell with 10 bars of syn gas slowly reversed this reaction. Heating this stirred mixture for about 2 h at 40 °C resulted in complete conversion to the active hydroformylation catalyst, $RhH(CO)_3P$, as was previously observed by Jongsma et al. [17] (ν_{CO} at 2093, 2043 and 2013 cm^{-1}). An additional amount of a decomposition product (2064, 2031 cm^{-1}) is detected as well. After addition of the less reactive internal alkene cyclohexene the carbonyl region of the IR spectrum remained unchanged. The infrared absorptions in the 2200–1600 cm^{-1} region that appear after shooting in the substrate are given in Table 2. During the catalytic reaction the absorptions remain the same with an additional band growing rapidly at approximately 1730 cm^{-1} originating from the product aldehydes. The data in the table show that the IR spectrum in the presence of cyclohexene is identical to that of $RhH(CO)_3P$ indicating that this is the resting state during the catalytic reaction. This is in accordance with the fact that the alkene addition to the hydrido complex is rate determining, as was pointed out by kinetic studies [16,17].

Table 2
Observed IR-frequencies in 2200–1600 cm^{-1} region after addition of substrate to $RhH(CO)_3P$ (P = tris(2-*tert*-butyl-4-methylphenyl) phosphite

Substrate	Observed frequencies (cm^{-1})
None	2093, 2043, 2013
Cyclohexene	2093, 2043, 2013
Oct-1-ene	2080, 2019, 1996, 1690[a]
Styrene	2080, 2022, 1998
Pentafluorostyrene	2079, 2027, 1998

[a] When performed with the rapid-scan method.

In the presence of 1-alkenes the IR spectra show a similar pattern in the carbonyl region as the spectrum of the $RhH(CO)_3P$ compound, but the ν_{CO} bands are shifted somewhat to lower energies. All signals are broad or contain a shoulder band. A possibly occurring metal-acyl frequency could not be observed with the used spectroscopic technique, owing to the immediate appearance of a strong overlapping absorption of the aldehyde product. Therefore, the experiment for oct-1-ene was repeated using the rapid-scan option where a sequence of spectra of up to 80 scans s^{-1} could be obtained. Figs. 2 and 3 shows a selection of the spectra of the two important frequency regions. Fig. 2 shows the section where the alkene and bridged CO vibrations are located, whereas Fig. 3 shows the metal-CO region. The difference in time between the first and the last shown spectrum is 0.82 s. An absorption at 1690 cm^{-1} is detected within 1 s and initially even two bands can be distinguished (Fig. 2). When the reaction proceeds, the aldehyde band appearing at 1734 cm^{-1} rapidly conceals both bands. After all the substrate was consumed, the spectrum belonging to the hydrido rhodium complex reappeared. In Fig. 3 the rapid conversion of the starting hydrido rhodium complex into the predominant species is depicted. The absorption patterns are shifted to lower frequencies, but similar to those of $RhH(CO)_3P$ indicating the presence of a complex with a structure analogous to the hydrido rhodium complex. The frequencies differ for the various substrates, which suggests that a substrate derived fragment is now coordinated to the rhodium. Migration of the hydride, subsequent to coordination of the alkene, can occur in two ways, one giving rise to the linear and the other to the branched alkyl rhodium intermediate. These and their derived compounds probably give rise to slightly different IR absorptions. This explains the broadness of the signals of the new species formed.

The reaction cycle of the rhodium-catalyzed hydroformylation consists of five substrate bonded intermediates (see Scheme 1): the π-coordinated alkene (**1**), the alkyl complexes $RhR(CO)_2P$ (**2**) and $RhR(CO)_3P$ (**3**), and the acyl complexes $RhC(O)R(CO)_2P$ (**4**) and $RhC(O)R(CO)_3P$ (**5**) (R = styryl, octyl or pentafluorostyryl) [15]. The coordinatively unsaturated complexes **2** and **4** are unlikely to have sufficiently long lifetime to be observed. Furthermore, three CO frequencies indicate that at least three CO molecules are coordinated to the rhodium, excluding **2** and **4** as the observed species. Rhodium carbonyl complexes without phos-

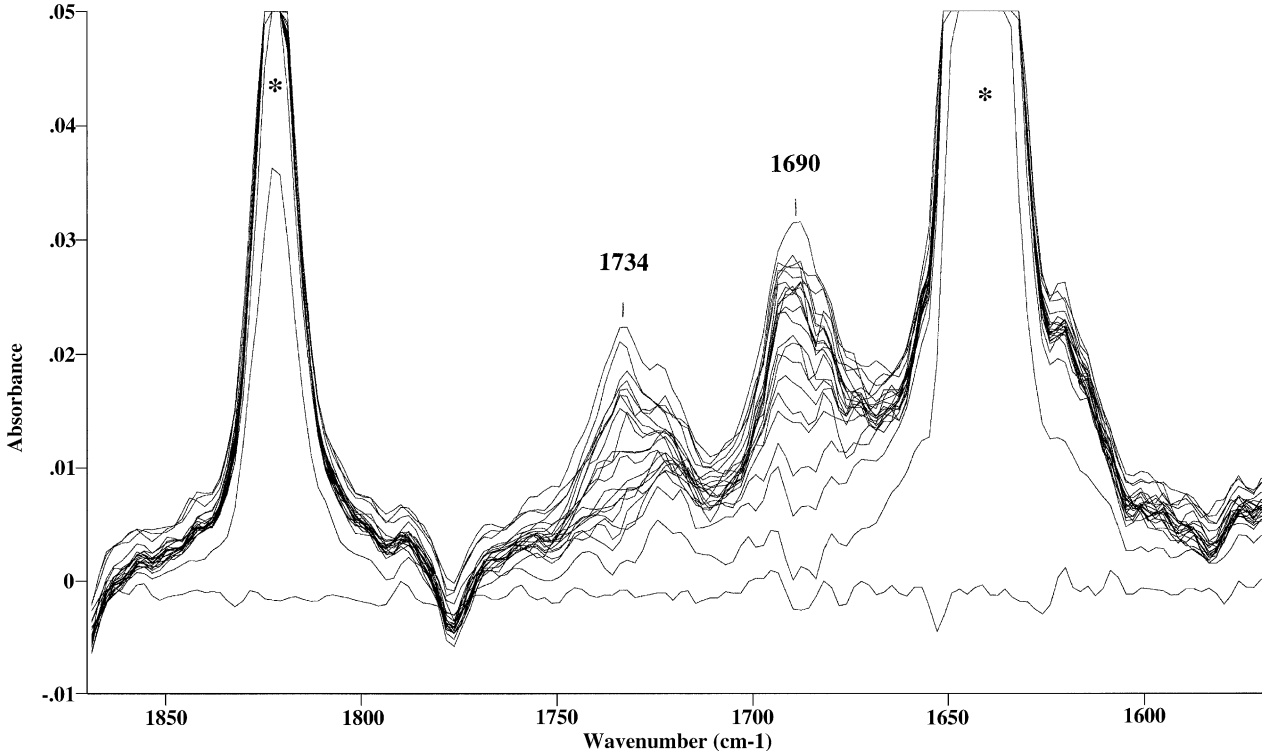

Fig. 2. Acyl region of IR spectra recorded with rapid-scan method after addition of oct-1-ene to RhH(CO)3P (P = tris(2-*tert*-butyl-4-methylphenyl) phosphite; * = oct-1-ene.

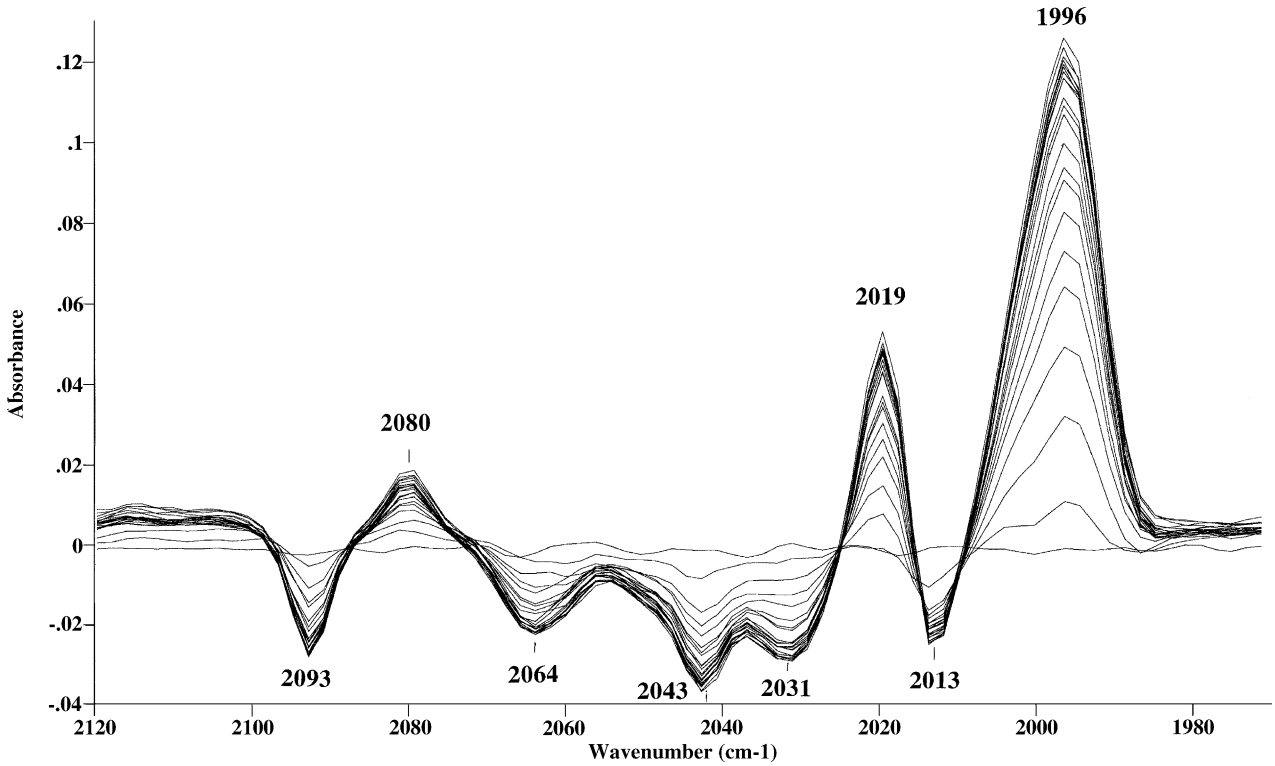

Fig. 3. Terminal CO region of IR spectra recorded with rapid-scan method after addition of oct-1-ene to RhH(CO)3P (P = tris(2-*tert*-butyl-4-methylphenyl) phosphite.

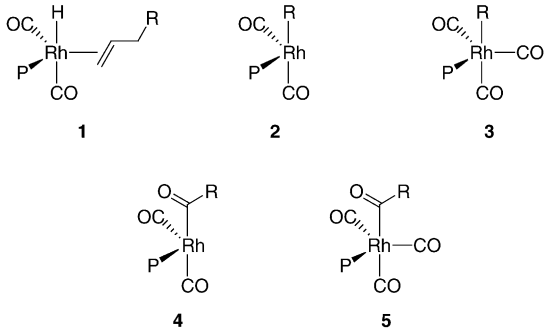

Scheme 1. Intermediates in the tris(2-*tert*-butyl-4-methylphenyl) phosphite modified rhodium catalyzed hydroformylation.

phorus ligands coordinated, have their ν_{CO}'s at substantially higher frequencies [15], excluding the phosphite as the substituted ligand. These considerations lead towards the coordinatively saturated complexes **3** and **5** as the possible most abundant species. Moreover, the additional CO absorption at 1690 cm^{-1} points into the direction of **5**. A CO band around 1700 cm^{-1} is characteristic of the CO stretch absorption of a keto-group [11]. Metal-acyl absorptions are usually very weak and broad, in accordance with our observations. Considering the steric hindrance that is caused on formation of the alkyl rhodium complex, **3**, a larger effect of the substrate on the CO frequencies would be expected. Besides, the absorption of especially the CO that is positioned trans towards the alkyl group would be strongly affected by the electronic influence of the different alkyl groups. The absence of this large substrate dependence indicates that **5** is the most likely species.

The presence of **5** as predominant species during the catalysis is also in accordance with the observed kinetic behavior of this catalyst with oct-1-ene and styrene as the substrates. The observation of this saturated acyl rhodium complex is in line with the negative dependence of the reaction rate on the CO concentration. As is discussed in a previous study [15] this saturated acyl complex is an unreactive "resting state". Before the final reaction step can occur, a CO molecule has to dissociate in order to form the coordinatively unsaturated complex, **4**. This means that **4** and **5** are in equilibrium and that their relative concentrations depend on the concentration of CO present in the reaction mixture.

3.2. Study of bulky phosphorus diamide ligands

N-acyl phosphorus diamides (**6**) provide a related class of bulky and strongly π-accepting ligands that show similar behavior in rhodium catalyzed hydroformylation as bulky phosphite. Similar to bulky phosphite the combination of electronic and steric ligand properties leads to an increase of the hydroformylation activity compared to phosphine-based catalyst systems [19]. The mechanism of the hydroformylation reaction has been investigated thoroughly by in situ identification of intermediate rhodium complexes and kinetic studies [20]. We studied the reaction mechanism using these phosphorus diamide ligands in order to understand the catalyst performance. The rate-limiting step in the hydroformylation reaction of 1-alkenes using ligand **6** was investigated and the solution structure of the resting state of the catalyst was studied using (in situ) high-pressure spectroscopic techniques.

The rhodium hydride as actual catalyst precursor was formed using $Rh(acac)(CO)_2$ in the presence of various concentrations of ligand under 20 bar of CO/H_2 (1/1). The reaction was monitored using high pressure (HP) NMR and HP IR spectroscopy in order to reveal the structure of these complexes. In all cases a mixture of $HRhL(CO)_3$ and $HRhL_2(CO)_2$ was observed with the ratio between $HRhL_2(CO)_2$ and $HRhL(CO)_3$ depending both on the ligand concentration and on the steric and electronic ligand

Table 3
NMR and IR data $HRhL_x(CO)_{(4-x)}$ (x = 1, 2 and 3) complexes (L = 6a–6d)

Compound	δ (^{31}P) (ppm)[a]	J_{RhP} (Hz)	δ (^{1}H) (ppm)[a]	ν_{CO} (cm^{-1})[b]
HRh**6a**$(CO)_3$	110	186	−10.6 (d, J_{PH}= 6 Hz)	2094, 2047, 2017
HRh(**6a**)$_2(CO)_2$	114	196	−11.4 (t, J_{PH}=12 Hz)	2079, 2023
HRh**6b**$(CO)_3$	104	177	−10.3 (d, J_{PH}=15Hz)	2095, 2045, 2008
HRh(**6b**)$_2(CO)_2$	110	181	−10.6 (s, broad)	2070, 2018
HRh(**6b**)$_3$CO	117	169	−10.7 (s, broad)	2019
HRh**6c**$(CO)_3$	Not observed		Not observed	2096, 2047, 2020
HRh(**6c**)$_2(CO)_2$	126	221	−10.6 (s, broad)	2071, 2003
HRh**6d**$(CO)_3$	116	220	Not observed	2098, 2043, 2014
HRh(**6d**)$_2(CO)_2$	118	224	−10.5 (s, broad)	2076, 2020

[a] Measured in toluene-d8.

[b] Complexes with L = **6a**, **6c** measured in 2-methyl tetrahydrofuran, complexes with L = **6b**, **6d** measured in cyclohexane.

properties. The spectroscopic data of the hydride complexes $HRhL_x(CO)_{4-x}$ (x = 1, 2 and 3) with ligands **6a–d** are presented in Table 3. A detailed kinetic study of the rhodium catalyzed hydroformylation of 1-octene using ligand **6b** resulted in the rate equation:

$$v = k[1-\text{octene}]^{0.3}[\mathbf{6b}]^{-0.3}[CO]^{-1}[Rh]^{1}[H_2]^{0.8}$$

The kinetic data show that the rate-determining step of the hydroformylation reaction using $HRh(CO)_2(\mathbf{6b})_2$ (**7b**, Scheme 2) cannot be reduced to one single step of the hydroformylation mechanism. Several reaction steps in the proposed mechanism are involved in the reaction rate control. The alkene coordination/hydride migration and the hydrogenolysis have similar rates and the overall reaction rate is strongly dependent of the conditions used. At high hydrogen pressure the alkene coordination/hydride migration determines the overall rate of the reaction and consequently the rhodium hydride is expected to be the most abundant species. When the alkene concentration is increased at relatively low hydrogen pressure the rate determining step shifts to the hydrogenolysis and as a result the rhodium acyl complex will be predominantly present.

Depending on the conditions both rhodium-hydride and rhodium-acyl complexes are expected to be present as potential "resting" states during the hydroformylation reaction. The complexes present were investigated using in situ spectroscopic techniques applying the IR autoclave. The results obtained in the in situ HP IR experiments are presented in Table 4. In a typical experiment the hydride complex **7b** was formed in situ and after addition of 1-octene the hydroformylation reaction was monitored using a rapid-scan IR technique (7 scans/s). The difference spectra obtained (Fig. 4) show negative absorption bands for the carbonyl frequencies of com-

Table 4
Absorptions obtained in in situ IR experiments

p_{CO} (bar)	p_{H_2} (bar)	[1-octene] (M)	ν_{CO} (cm^{-1})[a]	
			Disappearing[b]	Appearing[b]
7	7	0.2	2070 (**7b**)	2085 (w)
			2018 (**7b**)	2077 (sh)
				2028 (w)
				2010 (sh)
				2001 (m)
				1991 (m)
				1967 (w)
7	32	0.2	–[c]	–[c]
7	7	0.6	2070 (**7b**)	2085 (w)
			2018 (**7b**)	2077 (sh)
				2028 (w)
				2010 (sh)
				2001 (m)
				1991 (m)
				1967 (w)

[a] All experiments were performed in cyclohexane at 40 °C.
[b] Appearing absorption bands are obtained for carbonyl frequencies of complexes that are formed during the hydroformylation reaction, whereas disappearing absorption bands are obtained for carbonyl frequencies of complexes that are converted to other complexes.
[c] No change in IR spectrum was observed.

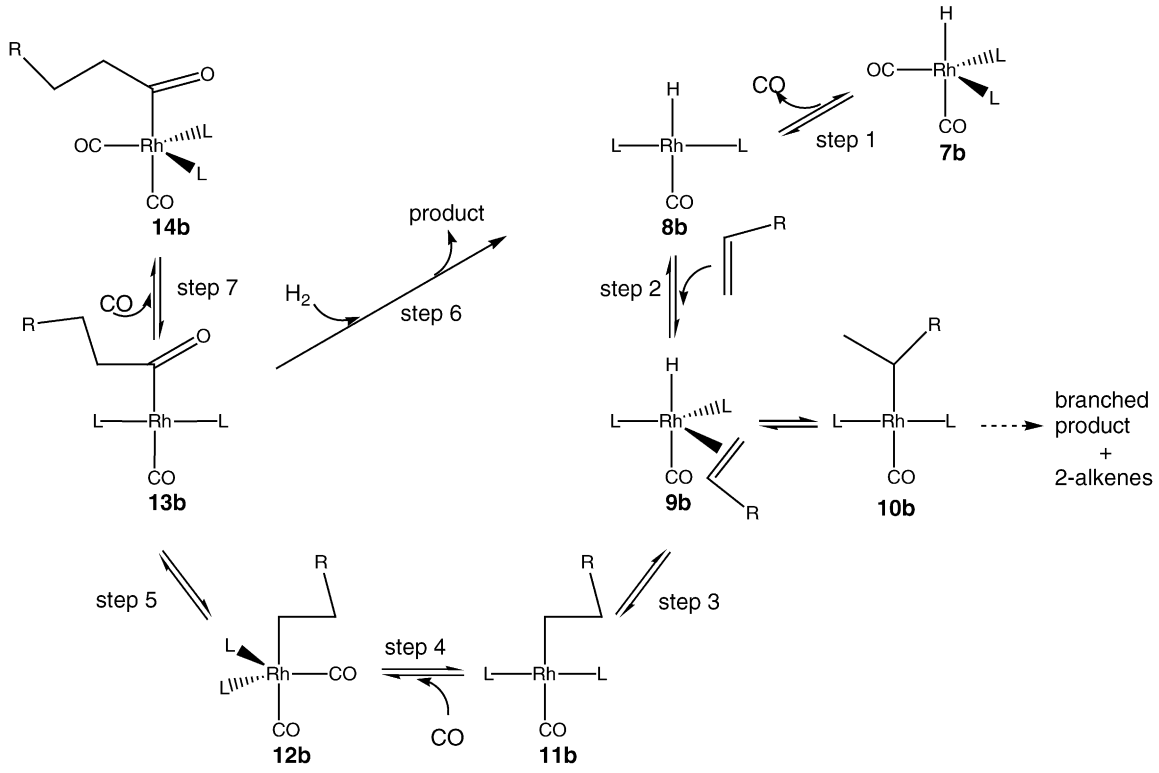

Scheme 2. Hydroformylation reaction cycle.

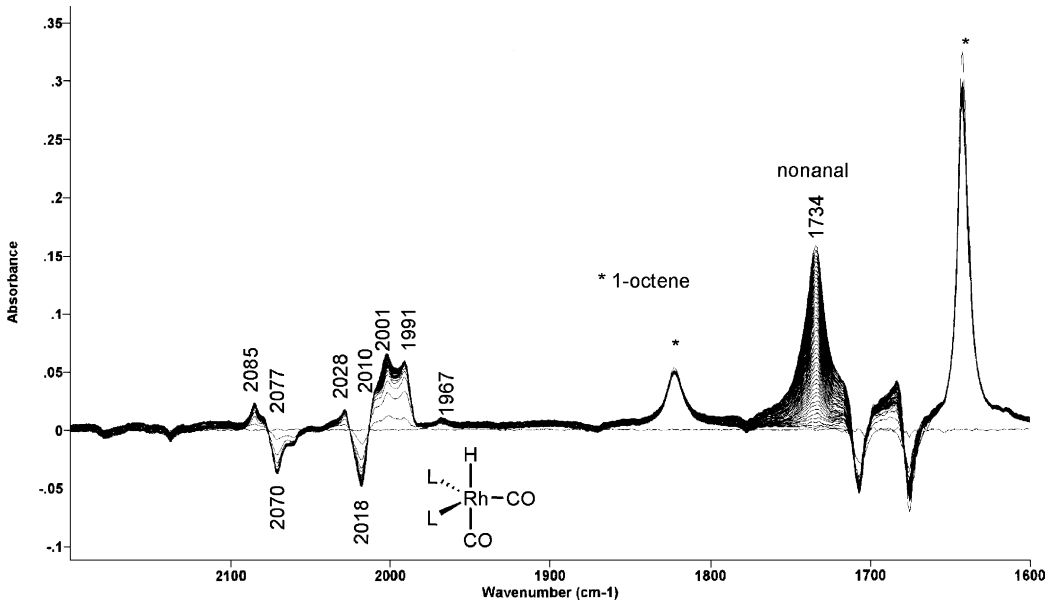

Fig. 4. Difference spectrum of the in situ IR experiment.

plexes that are converted (in part) to other complexes after addition of the substrate. Positive absorption bands are obtained for carbonyl frequencies of complexes that are formed during the hydroformylation reaction. The rhodium hydride complex **7b** (ν_{CO} = 2070 and 2018 cm^{-1}, Table 4) is the only rhodium complex present in all experiments before addition and after complete conversion of 1-octene. The difference IR spectra show absorption bands in the terminal carbonyl region only. No absorptions of bridging carbonyls are observed, which confirms that inactive rhodium dimers or clusters are not present during the reaction as already concluded from the first order rate-dependency on the rhodium concentration observed in the kinetic experiments.

Immediately after addition of 1-octene, the strong absorption band of nonanal (1734 cm^{-1}) appeared in the IR spectrum, proving that the hydroformylation reaction has started. The amount of **7b** dropped considerably upon addition of 1-octene. However, comparison of the intensities of the carbonyl frequencies of **7b** before and after addition of 1-octene showed that **7b** was still present in low concentration during the hydroformylation reaction. Seven new absorptions appeared in the terminal carbonyl region indicating that complex **7b** was converted (in part) to several new carbonyl containing rhodium complexes.

The kinetic experiments showed that the hydrogenolysis (step 6, Scheme 2) is a relatively slow step in the hydroformylation reaction and rhodium-acyl complexes will be present during the hydroformylation reaction. Several possible structures of rhodium-acyl complexes are depicted in Scheme 3. Since the catalyst does not show high selectivity towards the linear aldehyde it can be concluded that both the linear and branched rhodium-acyl complexes are formed (**14b**, **15b**). Coordination of one of the phosphorus atoms at an apical position leading to **ea** coordinated complexes is also possible. The new carbonyl bands obtained in the IR spectrum belong probably to several of the rhodium-acyl complexes as depicted in Scheme 3. The strong amide bands of the ligand in this region obscured the expected rhodium-acyl absorption band **15b** around 1600–1700 cm^{-1}. Therefore, in contrast to the bulky phosphite system, the rhodium acyl vibration could not be observed in the IR spectra.

Rhodium hydride complex **7b** was the only rhodium complex observed during the hydroformylation reaction at increased partial hydrogen pressure of 32 bars, as concluded from the absence of carbonyl signals in the IR difference spectra. The spectrum of the rhodium hydride resting state is taken as background at t = 0 (Table 4). The difference IR spectra show no terminal carbonyl bands indicating the presence of no other complex than rhodium hydride **7b** under these conditions. Higher hydrogen pressures facilitate the

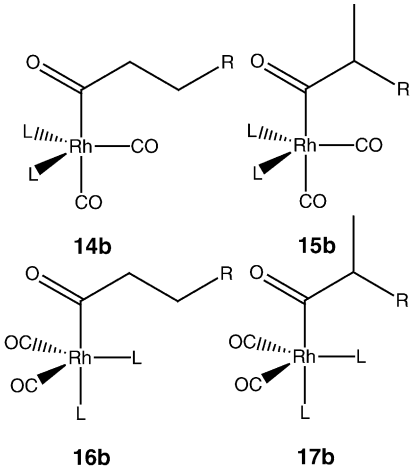

Scheme 3. Possible structures of rhodium acyl complexes.

Table 5
IR frequencies obtained in the stoichiometric reaction of **7b**, 1-octene, CO and H_2

Conditions[a]	ν_{CO} (cm^{-1})
7b under 5 bars of CO	2080, 2017
7b + 25 eq. of 1-octene under 5 bars of CO	2085 (w), 2077 (sh), 2028 (w), 2010 (sh), 2001 (m), 1991 (m) 1967 (w)
7b + 25 eq. of 1-octene under 10 bars of CO/H_2 = 1/1	2080, 2017

[a] All reactions were performed in cyclohexane at room temperature.

hydrogenolysis step and one of the early steps of the catalytic cycle becomes rate limiting. When the alkene concentration is raised, the amount of **7b** decreased and the intensity of the additional carbonyl bands increased. This indicates that the role of the hydrogenolysis reaction as rate-controlling step increases at higher alkene concentration. The shift of rate control between different steps depending on the conditions used shows that not one single step of the hydroformylation reaction determines the reaction rate. The rate expression of this catalyst system is strongly dependent on the conditions used.

A combination of HP NMR and IR studies was performed to reveal the occurrence of rhodium acyl intermediates. The hydroformylation reaction was investigated in a stepwise manner by the subsequent reactions of **7b** with alkene, CO, and H_2 in an attempt to characterize the complexes formed during the hydroformylation reaction. In the absence of H_2, complex **7b**, alkene and CO can undergo all hydroformylation reaction steps except for the hydrogenolysis step and rhodium-acyl complexes will be formed. The IR data obtained after the subsequent reaction steps are presented in Table 5. The carbonyl frequencies obtained after the reaction of **7b**, 1-octene and CO are identical to those obtained in the in situ IR experiments obtained during the hydroformylation reaction except for the carbonyl frequency due to the aldehyde. Subsequent addition of hydrogen showed aldehyde formation and when all 1-octene was converted, **7b** was the only complex present. Therefore we concluded that the complexes formed in the stoichiometric reaction of **7b**, alkene and CO are equal to the most abundant complexes present during the hydroformylation reaction at low H_2 pressure. This indicates that the stoichiometric reaction is an elegant and reliable method to study the intermediates of the hydroformylation reaction in a stationary system.

In addition the stoichiometric hydroformylation of 1-hexene using NMR spectroscopy was investigated using the same procedure as that for the IR experiments. The experiments were performed in a high pressure NMR flow cell as described by Iggo et al. [9]. The advantages of a HP flow cell instead of a HP NMR tube [21] are the continuous supply of reactants and optimal mixing of the reactants (minimization of diffusion problems). Homogeneously catalyzed reactions can be monitored using this flow cell and stable intermediates can be characterized using different NMR techniques.

Rhodium complex **7b** was prepared in situ in the NMR cell from $Rh(acac)(CO)_2$ and 5 equivalents of ligand **6b** at 80 °C under 20 bars of CO/H_2 = 1/1 (spectrum a, Fig. 5). Complex **7b** is the only rhodium complex obtained according to the ^{31}P NMR spectrum. After removal of hydrogen gas by bubbling CO through the solution for 30 min approximately 25 equivalents of 1-hexene were injected into the NMR cell at 253 K. Upon warming to room temperature, the ^{31}P NMR spectrum started to broaden and both the ^{1}H NMR and ^{31}P NMR spectrum showed that the resonance due to the hydride complex decreased in intensity. After decreasing the temperature to 253 K the spectrum showed an additional (broad) doublet (δ = 109.5 ppm, J_{RhP} = 205 Hz) upfield from the doublet of **7b** (spectrum b, Fig. 5). Complex **7b** was converted almost completely to the new compounds by warming the solution to room temperature again (spectrum c, Fig. 5). A broad resonance appeared downfield from the doublet indicating that probably more than one complex is present. The ^{31}P NMR spectrum at room temperature showed a very broad peak at the position of the free ligand (64 ppm) indicating that the coordinated phosphorus ligands were in exchange with the free phosphorus ligand. The hydride resonance in the ^{1}H NMR spectrum had disappeared and no aldehyde resonance was observed.

Changing the gas flow to 5 bars of CO/H_2 (1/1) resulted in reformation of the hydride complex **7b** (spectrum d, Fig. 5). The ^{1}H NMR spectrum showed the reappearance of the hydride resonance at −10.6 ppm together with an aldehyde resonance at 9.3 ppm. Repeating this sequential procedure with this NMR sample gave the same results, confirming that the complex formed in absence of H_2 is an intermediate of the hydroformylation reaction.

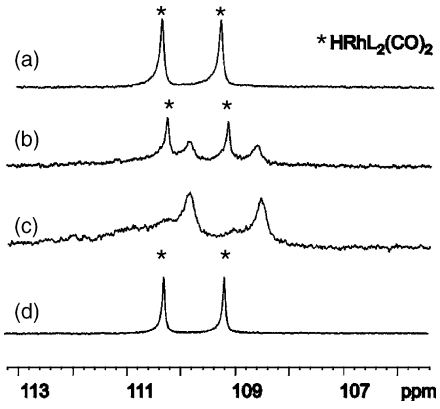

Fig. 5. Overview of the $^{31}P\{^{1}H\}$ NMR spectra of stepwise reaction of **7b**, 1-hexene and CO and H_2, all spectra were recorded at 253 K: (a) $^{31}P\{^{1}H\}$ NMR spectrum of **7b** under 5 bars of CO; (b) $^{31}P\{^{1}H\}$ NMR spectrum of **7b** in presence of 5 bars of CO and 25 eq. of 1-hexene. Approximately 50% of **7b** was converted to a new rhodium complex: (c) $^{31}P\{^{1}H\}$ NMR spectrum after complete conversion of **7b** to a new rhodium complex; (d) $^{31}P\{^{1}H\}$ NMR spectrum after addition of 5 bars of CO/H_2 (1/1) to the solution. Reproduced from reference [20] with permission.

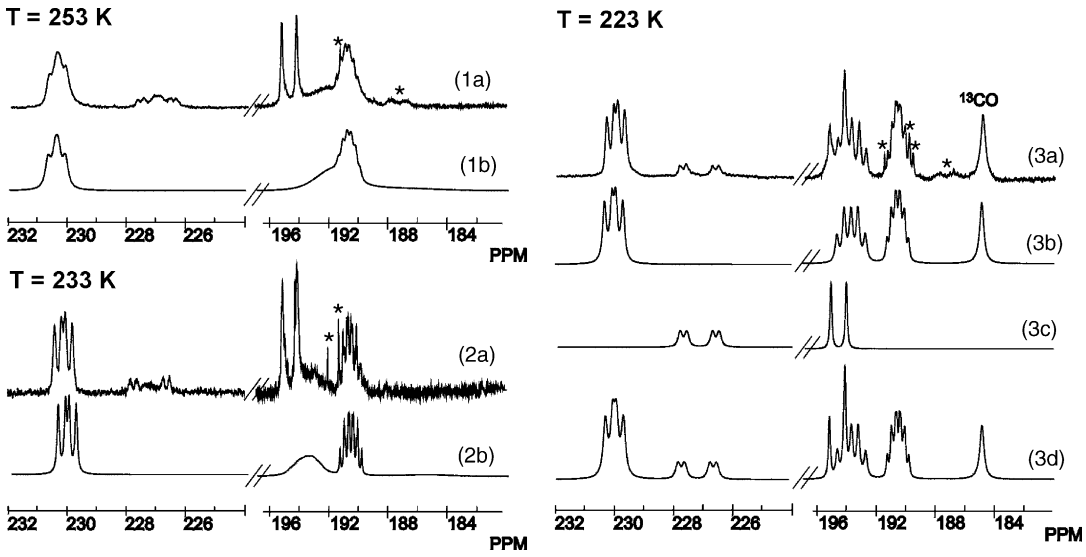

Fig. 6. Variable temperature $^{13}C\{^1H\}$ NMR spectra obtained after the reaction of 7b, 1-hexene at CO (1a) $^{13}C\{^1H\}$ NMR spectrum obtained at 253 K; (1b) Simulation of $^{13}C\{^1H\}$ NMR spectrum 1a; (2a) $^{13}C\{^1H\}$ NMR spectrum obtained at 223 K; (2b) Simulation of $^{13}C\{^1H\}$ NMR spectrum 2a; (3a) $^{13}C\{^1H\}$ NMR spectrum obtained at 223 K; (3b) simulation of the $^{13}C\{^1H\}$ NMR spectrum of **14b/15b** at 223 K; (3c) simulation of the $^{13}C\{^1H\}$ NMR spectrum of **16b/17b** at 223 K; (3d) Simulation $^{13}C\{^1H\}$ NMR spectrum obtained at 223 K; *: impurity. Reproduced from reference [20] with permission.

The reaction was also performed with ^{13}CO to be able to identify the rhodium-acyl resonance in ^{13}C NMR. All resonances obtained in the ^{13}C NMR spectrum are very broad at room temperature. The resonances sharpened when the temperature was decreased (Fig. 6). The ^{13}C NMR spectrum at 223 K (Spectrum 3a, Fig. 6) showed two rhodium acyl resonances (δ = 230.0 and 227.2 ppm) and three different rhodium carbonyl resonances (δ = 194.7, 193.7 and 190.6 ppm) indicating that we are dealing with two different rhodium acyl complexes.

The structure of the two rhodium acyl complexes was elucidated using ^{13}C COSY90 spectra, selective decoupling of the phosphorus resonances, and ^{103}Rh-^{13}C HMQC spectra. Spectrum 3d (Fig. 6) shows the complete simulation of the $^{13}C\{^1H\}$ NMR spectrum obtained at 223 K. The $^{13}C\{^1H\}$ NMR spectrum contains both rhodium acyl complexes **14b/15b** en **16b/17b** in a ratio 1–0.4. Both rhodium acyl complexes have a trigonal bipyramidal structure with the acyl moiety coordinated at an apical position. Both complexes contain two phosphorus ligands and two carbonyl ligands. The major complex formed contains two phosphorus ligands coordinated in the equatorial plane of the trigonal bipyramid, the minor complex has probably one phosphorus atom coordinated at an equatorial position, one at an apical position of the trigonal bipyramid. We are not able to distinguish between the linear and branched acyl structure based on the NMR data obtained.

3.3. Study of elementary steps of the catalytic cycle

3.3.1. CO-dissociation

Casey and Whiteker introduced the concept of the natural bite angle to calculate the preferred chelation angle of diphosphine ligands using molecular mechanics [22]. They were the first to show that the bite angle has a great influence on the regioselectivity in the rhodium-catalyzed hydroformylation [23]. Following this approach we have developed a series of diphosphine ligands based on the xanthene-type backbones (Fig. 7) [24,25]. In this series of ligands, a clear trend of increasing selectivity for linear aldehyde formation with increasing natural bite angle was observed. We discovered that not only the variation of the ligand backbone but also substitution of the standard diphenylphosphine moieties has a direct influence on the ligand bite angle. We developed new phosphacyclic xantphos derivatives that have shown an increased preference for **ee** coordination and display a higher activity in the hydroformylation of 1-octene than the non-cyclic parent ligand. Moreover, DBP-xantphos (**19**) and POP-xantphos (**22**) give very active and selective catalysts for the hydroformylation of internal octenes to linear nonanal [26,27].

To investigate the origin of the very high hydroformylation and isomerization activity of ligand **22** we measured the rate of CO dissociation from the (diphosphine)$Rh(CO)_2H$ complex using ^{13}CO labeling in rapid-scan IR experiments [27]. The CO dissociation rate constants k_1 can be obtained by exchanging ^{13}CO for ^{12}CO in the (diphosphine)$Rh(^{13}CO)_2H$ complexes [9]. The CO dissociation proceeds via a dissociative mechanism and consequently obeys simple first-order kinetics. The rate constants k_1 can, therefore, be derived from Eqs. (1) and (2).

$$-\mathrm{d}[(\text{diphosphine})\mathrm{Rh}(^{13}\mathrm{CO})_2\mathrm{H})]/\mathrm{d}t = k_1[(\text{diphosphine})\mathrm{Rh}(^{13}\mathrm{CO})_2\mathrm{H})] \quad (1)$$

$$\ln[(\text{diphosphine})\mathrm{Rh}(^{13}\mathrm{CO})_2\mathrm{H})] = -k_1 t + \ln[(\text{diphosphine})\mathrm{Rh}(^{13}\mathrm{CO})_2\mathrm{H})]_0 \quad (2)$$

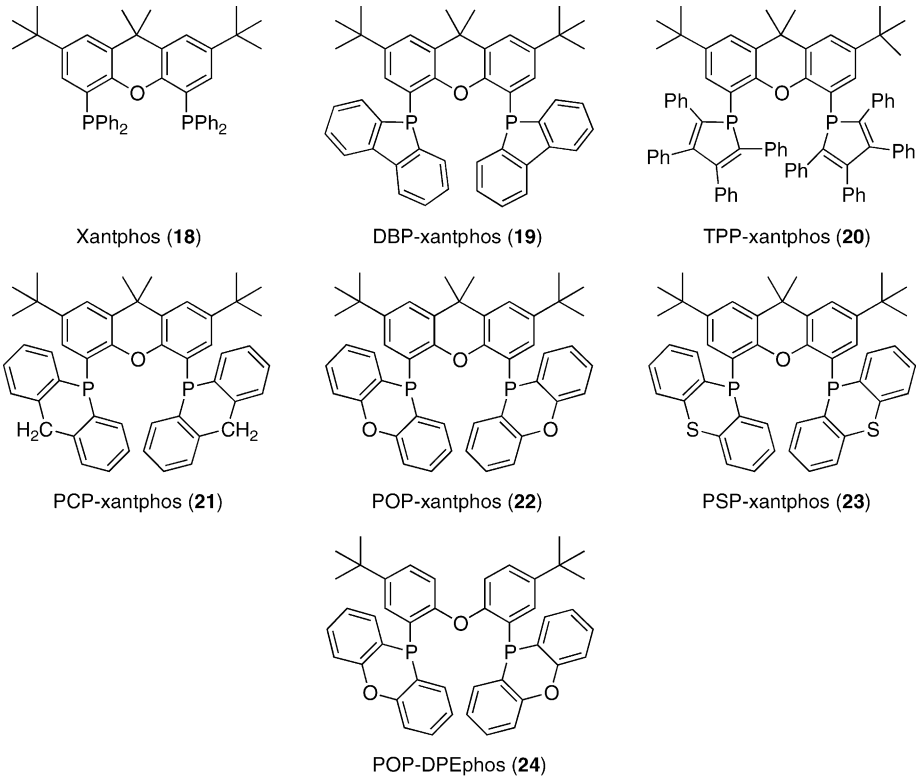

Fig. 7. Xantphos family.

The (diphosphine)Rh(^{13}CO)$_2$H complexes were prepared in situ from Rh(acac)(CO)$_2$ and diphosphine under an atmosphere of ^{13}CO/H$_2$ (1:4). The exchange of ^{13}CO for ^{12}CO in the (diphosphine)Rh(^{13}CO)$_2$H complexes was monitored by rapid-scan HP IR spectroscopy at 40 °C. The ^{13}CO/^{12}CO exchange was initiated by adding a large excess of ^{12}CO. The carbonyl absorptions of the complexes at approximately 1945 cm^{-1} (1948 cm^{-1} for ligand **22**, see Fig. 8a) were taken to calculate the concentrations of the complexes. These absorption bands are assigned to one of the CO vibrations of the **ee** isomer of the complexes. Representative kinetic data of the experiments with ligand **21** and **22** are shown in Fig. 8, and the observed rate constants, k_1, are listed in Table 6.

The representative difference IR spectrum displayed in Fig. 8a for one of the experiments with (**22**)Rh(^{13}CO)$_2$H (**25-^{13}CO**) clearly shows the conversion of the ^{13}CO labeled complex in to its ^{12}CO analogue **25-^{12}CO**. In the IR spectrum only the **ee** complex isomer is visible (vide supra). The exponential decay of the intensity of the carbonyl absorption at 1948 cm^{-1} in time is displayed in Fig. 8b and the linear plot of the natural logarithm of the complex concentration (ln[Rh]) versus time in Fig. 8c. The negative of the slope of this line is the first-order rate constant k_1 (Eq. (2)).

Table 6
Kinetics ^{13}CO dissociation (diphosphine)Rh(^{13}CO)$_2$H complexes[a]

Ligand	Phosphacycle	P (CO) (bar)	r^2	k_1 (h^{-1})
21	Phosphorine	25	0.987	−288 ± 8
21		25	0.987	−266 ± 7
22	Phenoxaphosphine	25	0.992	−1188 ± 29
22		25	0.990	−1171 ± 23

[a] Reaction conditions: [(diphosphine)Rh(^{13}CO)$_2$H] = 2.00 mM in cyclohexane, P(^{13}CO) = 1 bar, P(H$_2$) = 4 bar, T = 40 °C, diphosphine/Rh = 5. Values for k_1 are least-squares fit of lines from ln[Rh] vs. time over the first 15 s (ligand **21**) or over the first 4 s (ligand **22**).

The decay of the carbonyl resonances of the (diphosphine)Rh(^{13}CO)$_2$H complexes in time follows simple first-order kinetics in all experiments. Plots of the ln[(diphosphine)Rh(^{13}CO)$_2$H)] versus time are linear for at least two half-lives. Comparison of the rate constants k_1 obtained for ligands **21** and **22** [27] with the ones obtained for other xantphos ligands [25], shows that the CO dissociation rate for ligand **21** is in the same range as other ligands. The CO dissociation rate for ligand **22**, however, proves to be four to six times as high.

Furthermore, the rate is also independent of the (diphosphine) Rh(^{13}CO)$_2$H complex concentration, as demonstrated by the experiments with ligand **21**. It can therefore be concluded that the CO dissociation for these complexes proceeds by a purely dissociative mechanism and obeys a first-order rate-law. The observed k_1 values for the wide bite angle ligands revealed that the rates of CO dissociation, measured at 40 °C, are higher than the hydroformylation rates at 80 °C [24,26]. Since reaction rates increase approximately an order of magnitude with a temperature rise of 20 degrees, the CO

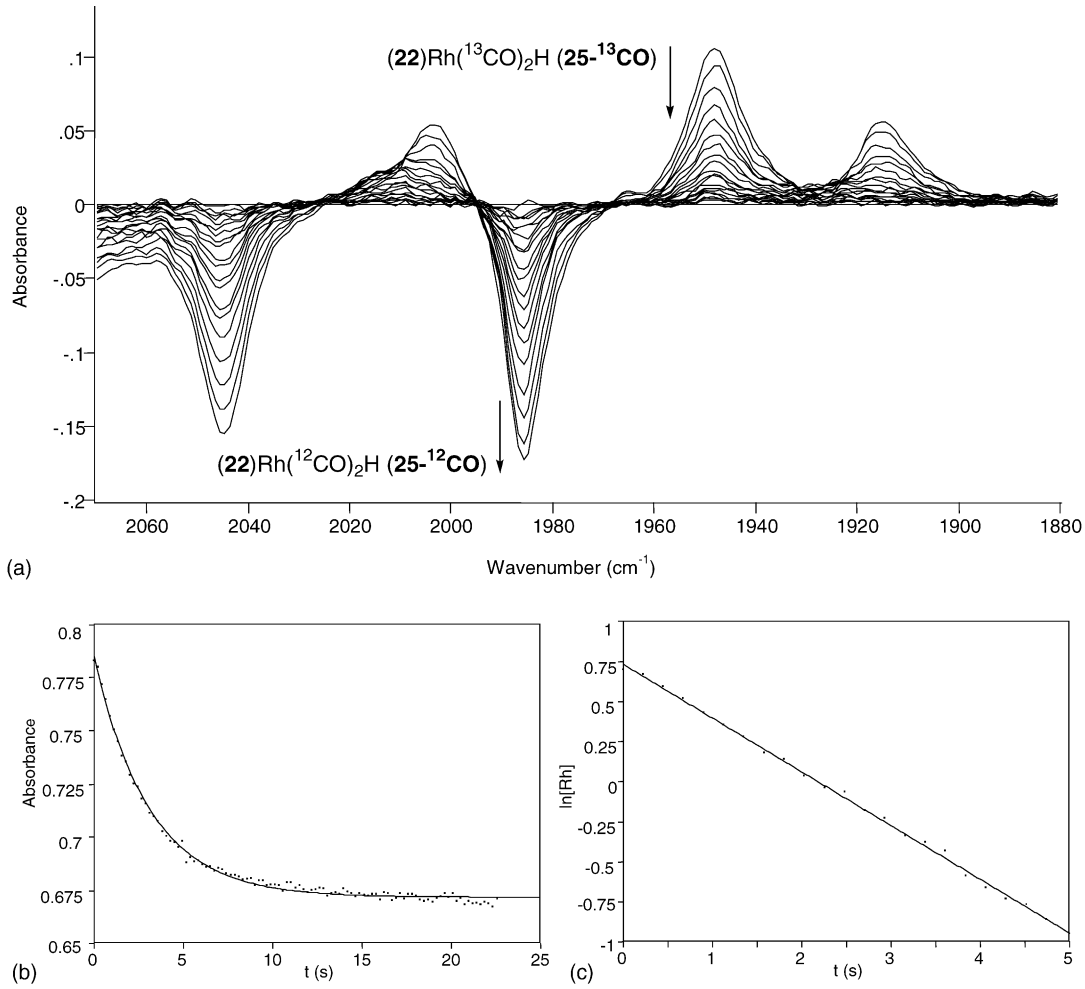

Fig. 8. Representative difference IR spectrum (a) and kinetic data (b and c) for the ^{13}CO dissociation from (**22**)Rh($^{13}CO)_2$H (**25**-^{13}CO) in the presence of unlabeled CO at 40 °C. Reproduced from reference [27] with permission.

dissociation rate at 80 °C is about 100 times as fast as the hydroformylation reaction.

3.3.2. *Exchange between RhD and H_2*

Important mechanistic information on the hydroformylation reaction can be obtained by deuterium labeling studies. The outcome of these labeling studies, however, will be influenced if fast exchange between rhodium hydrides (or deuterides) and bulk H_2 (or D_2) occurs. Therefore, we studied the H/D exchange rate of a catalyst system based on a π-acidic phosphorusdiamide ligand (**26**) in the absence of substrate using rapid-scan IR spectroscopy [28].

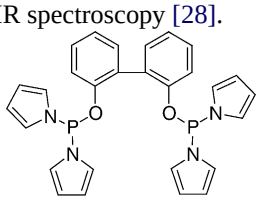

26

The IR absorptions of the carbonyl ligands of a rhodium-deuteride and a rhodium-hydride complex differ significantly for rhodium complexes containing two phosphorus ligands in the equatorial plane (Table 7). For the investigation of the H/D exchange rate, we synthesized DRh(**26**)$(CO)_2$ in situ from Rh(acac)$(CO)_2$ and 1.5 equivalents of ligand **26** under 20 bar of CO/D_2 (1/1). After complete conversion to the deuteride complex, the D_2 gas was removed by flushing several times with 5 bar of carbon monoxide. The H/D exchange was initiated by adding 10 bar of hydrogen to DRh(**26**)$(CO)_2$ under 10 bar of carbon monoxide. The exchange process was monitored using rapid-scan high-pressure IR spectroscopy at 80 °C (1.3 spectra s^{-1}). The difference IR spectrum presented in Fig. 9 shows that the rhodium-deuteride complexes DRh(**26**)$(CO)_2$ and DRh(**26**)$_2$(CO) (negative peaks at ν_{CO} = 2067, 2041 and 2020 cm^{-1}) are quantitatively converted into the rhodium-hydride complex HRh(**26**)$(CO)_2$ (positive peaks at ν_{CO} = 2078 and 2026 cm^{-1}). The presence of small amounts of HRh(**26**)$_2$(CO) could not be determined because of overlap with one of the absorptions of the deuteride complex.

The exponential decay of the strongest carbonyl absorption is presented in Fig. 10a (ν_{CO} = 2020 cm^{-1}). The maxi-

Table 7
Spectroscopic data of $HRh(L)_x(CO)_{4-x}$ complexes (x = 2, 3 and 4)

Complex	δ (^{1}H) (ppm)[a]	δ (^{31}P) (ppm)[a]	J_{HP} (Hz)	J_{HRh} (Hz)	J_{RhP} (Hz)	ν_{CO} (cm^{-1})[b]
HRh(**26**)$(CO)_2$)	−10.7 (broad)	138				2078, 2026
DRh(**26**)$(CO)_2$						2067, 2020
HRh(**26**)$_2$(CO)	−10.5 (broad q)[c]	135 (m)	6	≤3	nd[e]	2069
		111 (s)[d]				
DRh(**26**)$_2$(CO)						2041
		115 (s)[d]				
			36			
HRh(**26**)$_2$	−10.9 (dqui)	129	36	6	203	–
	−10.3 (dqui)	130		6	203	–

[a] Measured in toluene-d_8 or benzene-d_6.
[b] Measured in cyclohexane.
[c] All phosphorus atoms have similar J_{HP} coupling constants; q = quartet, qui = quintet.
[d] This chemical shift belongs to the non-coordinated phosphorus atom of (L ∩ L′).
[e] Not determined.

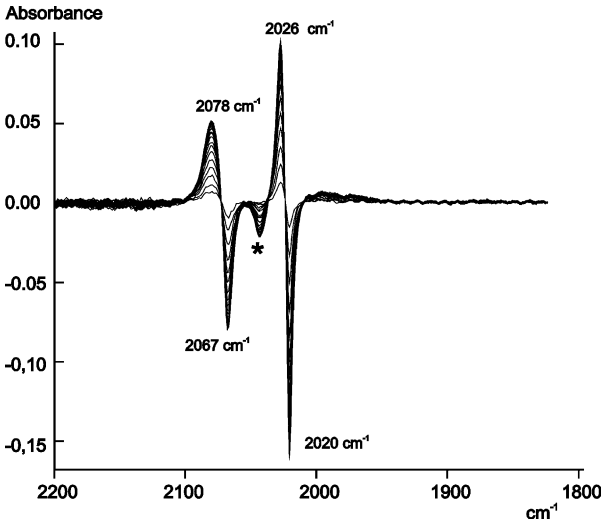

Fig. 9. Difference IR spectrum obtained after addition of H_2 to a solution of DRh(**26**)$(CO)_2$ and DRh(**26**)$_2$(CO) (indicated by *) under carbon monoxide pressure at 80 °C. Reproduced from reference [28] with permission.

mum absorbance of this frequency was taken as 100%. The natural logarithm of the relative absorption of the carbonyl frequency at 2020 cm^{-1} versus time is presented in Fig. 10b. The decay of the carbonyl frequency of the deuteride complex showed first order kinetics in the rhodium concentration and the pressure of H_2 and a H/D exchange rate of 1140 h^{-1} was calculated. Although the H/D exchange reaction was very fast

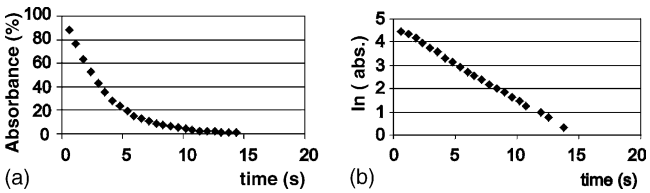

Fig. 10. Kinetic data of the H/D exchange: (A) exponential decay of ν_{CO} at 2020 cm^{-1} vs. time. (B) Logarithmic plot of the decay of the relative absorption at 2020 cm^{-1} vs. time. Reproduced from reference [28] with permission.

indeed, the initial rate of hydroformylation of 10×10^3 mol aldehyde (mol Rh h)$^{-1}$ with this catalyst was still an order of magnitude higher. This implied that up to 70% conversion of alkene RhH/D_2 exchange is not significant with this catalyst system. At high conversion the rate of hydroformylation is lower, because of the first-order dependence in the alkene concentration, and therefore some H/D exchange will occur.

3.4. Catalyst deactivation

The stability, deactivation [29] and regeneration of the catalyst are, next to activity and selectivity, important issues in homogeneous catalysis. The TON of a catalyst, a reflection of the catalyst stability, is one of the pivotal parameters for implementation of an actual process. Deactivation can occur in many ways, but sometimes deactivation is temporary only and the catalyst activity is restored. For long-term catalyst performance in the hydroformylation reaction, avoiding deactivation of the catalyst caused by reactive impurities in alkene feeds is of great importance. Such impurities may trap active rhodium catalysts either in a temporary or a permanent inactive state. It is known [29] that dienes and alkynes are poisons for many catalytic processes involving alkenes. Since hydroformylation of dienes is much slower than that of alkenes [30], diene impurities might slow down 1-alkene hydroformylation, depending on the resting state of the catalytic cycle of the diene [31]. Examples of such deactivation have also been reported in patent literature [32].

To obtain a better understanding of catalyst decomposition processes we have studied the deactivation of hydroformylation catalysts by controlled reaction with the most likely impurities in alkene feeds, such as dienes, alkynes and enones [33]. The hydrido rhodium complex $HRh(CO)_2(PPh_3)_2$ (**27**), the common resting state in hydroformylation, at which the catalytic cycle starts, was prepared in an HP-IR autoclave. Addition of unsaturated ketones, such as 3-buten-2-one (MVK, **28**) to a solution of $HRh(CO)_2(PPh_3)_2$ (**27**) immediately gave two new bands in the IR spectrum (Table 8) and disappearance of the four bands characteristic

Table 8
Influence of poisons/inhibitors on the Rh-CO bands of **27**

27 + poison/inhibitor	Rh-CO bands (cm^{-1})
–	1953, 1986, 1997, 2043
2,4-Hexadiene	1967, 2016
1,3-Pentadiene	1949 (w), 1957 (s), 2016 (s)
1-Octyne	1946, 1988, 2020, 2042, 2073, 2120
trans-3-Nonen-2-one	1946 (w), 1984 (vs)
3-Buten-2-one (MVK, **28**)	1946 (w), 1984 (vs)

of $HRh(CO)_2(PPh_3)_2$ (**27**) was observed (Fig. 11). Interestingly, when most of **28** had reacted, $HRh(CO)_2(PPh_3)_2$ (**27**) was regenerated and became again the predominant species.

We set out to characterize the product formed from $HRh(CO)_2(PPh_3)_2$ and **28** discussed above. HP ^1H and ^{31}P NMR spectroscopy was employed to study the intermediate products. As a model catalyst we used $RhH(CO)(PPh_3)_3$ (**29**) in the reaction with **28** in a ratio of 1:1.2. The NMR tube was cooled to −60 °C and ^1H, COSY, $^{31}P\{^1H\}$ and $^{13}C\{^1H\}$ NMR spectra were recorded. ^{31}P NMR showed complete conversion of $HRh(CO)(PPh_3)_3$ and two new doublets at 26.74 and 29.99 ppm and one molecule of free PPh_3 at −6.26 ppm were observed, indicating the formation of two isomeric insertion products. Their structure was unambiguously determined by in situ NMR spectroscopy. Two η^1 oxygen-bound rhodium enolate complexes (**30a** and **30b**) were identified and characterized also by IR spectroscopy giving a carbonyl signal at 1968 cm^{-1} (Scheme 4). The two characteristic IR frequencies of **28** at 1690 and 1719 cm^{-1} had disappeared.

When the reaction of **29** with **28** was complete and a mixture of the two isomers **30a** and **30b** was formed, CO/H_2 or CO was bubbled through the reaction mixture for 6 min at −60 °C. ^1H and $^{31}P\{^1H\}$ spectra taken after the reaction showed complete conversion of **30** and formation of new species, which we characterized using HP IR and several NMR techniques (**31**, Scheme 4). ^1H NMR spectroscopy showed formation of two carboalkoxyrhodium complexes, existing as a mixture of E/Z isomers (**31a** and **31b**) in a ratio of 30:70. Structurally analogous carboalkoxy complexes of iridium, which are formed upon carbonylation of four-coordinate iridium alkoxides, have been reported [34].

The reaction of **30** with CO was also performed in the HP IR autoclave. When **28** was added to a cyclohexane solution of **29** the bands in the IR spectrum characteristic of the rhodium hydride complex (2011 and 1938 cm^{-1}) disappeared and a new band characteristic of **30** appeared at 1968 cm^{-1}. Then CO/H_2 or CO was added to the reaction mixture and the latter band disappeared and new bands at 1984 and 1946 cm^{-1} were observed, indicative of two coordinated carbonyl ligands. The positions of these bands in the IR spectrum were exactly the same as those observed earlier after addition of **28** to the solution of **27** under CO/H_2 condition (Fig. 11).

The formation of **31** is the cause for slow or no hydroformylation of 1-octene when **28** is present in the reaction mixture. The unsaturated ketone is much more reactive toward **27** than the alkene and forms carboalkoxy complexes with rhodium thus blocking its activity for the 1-octene hydroformylation. Catalyst **27** for the hydroformylation of 1-octene is only restored after the enone has been converted to 2-butanone. The formation of formate esters from the enone substrate was not observed by GC-MS and HP NMR spectroscopy. The analysis of the reaction mixture confirmed that the only organic product present after the reaction was 2-butanone. The rhodium enolate complexes react very fast with CO leading to the formation of **31**, which does not react with H_2 as formate formation is apparently very slow.

Instead, a deinsertion has to occur to allow for hydrogenation of **30**, resulting in butanone formation. In equilibrium, during a catalytic reaction, the concentration of **30** is too low to observe using HP IR spectroscopy. When most of **28** has been converted to butanone, the hydroformylation of 1-octene can proceed (Scheme 4).

4. Cobalt catalyzed hydroformylation

The great advantage of the HP-IR cell is that it allows mechanistic studies under actual catalytic conditions. This

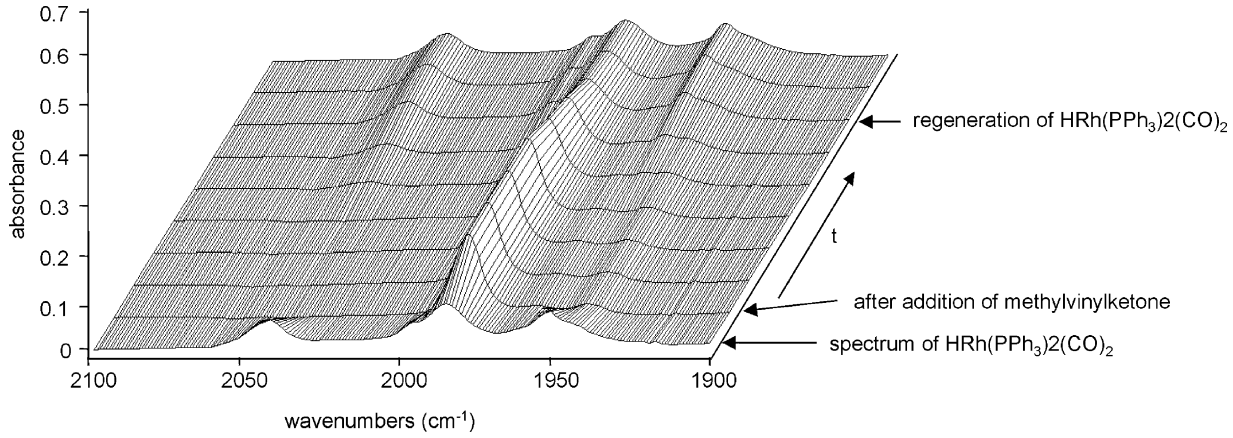

Fig. 11. In situ HP IR study of the reaction of **27** with **28**. Reproduce from reference [33] with permission.

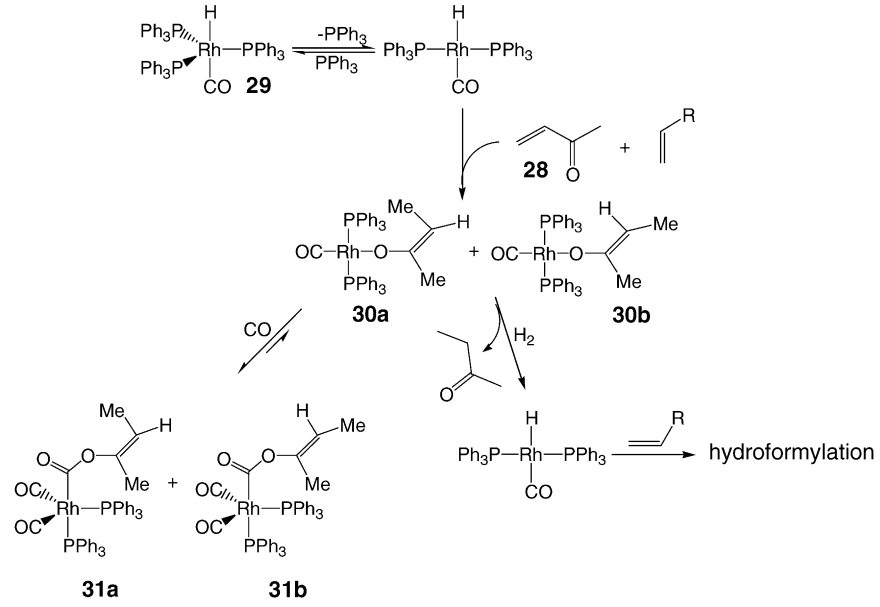

Scheme 4.

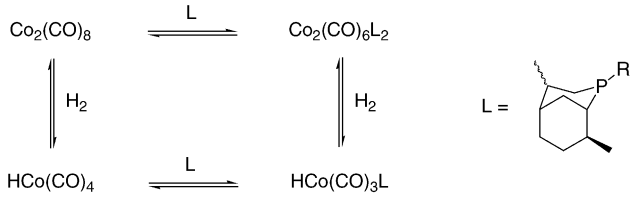

Scheme 5. Equilibrium of cobalt complexes under hydroformylation conditions.

has been exploited by Crause et al. at Sasol in an elegant mechanistic study of the formation of the catalytically active phosphine modified cobalt hydride from the dicobalt octacarbonyl precursor [35]. They showed that the activity and selectivity of the hydroformylation of 1-dodecene was mainly governed by the equilibrium between the modified and unmodified cobalt species under the applied reaction conditions (Scheme 5).

In conclusion, the newly developed in situ IR autoclave is highly suitable for following very fast catalytic reactions such as the hydroformylation reactions described. With the use of this autoclave the rapid-scan IR technique can provide detailed mechanistic information. By making use of isotopic labeling it is possible to study individual elementary reaction steps of a catalytic cycle.

Acknowledgments

We are grateful to Mr. J. Zoutberg and Mr. D.P. de Zwarte for the construction of the HP-IR cell and to Mr. M.M. Groeneveld for manufacturing the IR windows. We want to acknowledge the coworkers mentioned in the references, which were involved in the described mechanistic studies.

References

[1] P.W.N.M. van Leeuwen, C. Claver (Eds.), Rhodium Catalyzed Hydroformylation, Kluwer Academics Publishers, Dordrecht, 2000.
[2] J.F. Young, J.A. Osborn, F.A. Jardine, G. Wilkinson, J. Chem. Soc., Chem. Commun. (1965) 131.
[3] W. Strohmeier, F.J. Müller, Chem. Ber. 100 (1967) 2812.
[4] C.A. Tolman, Chem. Rev. 77 (1977) 313.
[5] C.P. Casey, G.T. Whiteker, Isr. J. Chem. 30 (1990) 299.
[6] G.W. Parshall, Homogeneous Catalysis: The Applications and Chemistry of Catalysis by Soluble Transition Metal Complexes, Wiley, New York, 1980.
[7] (a) P.W.N.M. van Leeuwen, K. Morokuma, J.H. van Lenthe (Eds.), Theoretical Aspects of Homogeneous Catalysis, Applications of Ab Initio Molecular Orbital Theory, Kluwer Academic Publishers, Dordrecht, 1995;
(b) F. Maseras, A., Lledós (Eds.), Computaional Modeling of Homogeneous Catalysis, Kluwer Academic Publishers, Dordrecht, 2002.
[8] (a) D.C. Roe, J. Magn. Res. 63 (1985) 388;
(b) I. Horvath, Organometallics 5 (1986) 2333.
[9] J.A. Iggo, D. Shirley, N.C. Tong, New J. Chem. (1998) 1043.
[10] (a) W. Rigby, R.W. Whyman, K. Wilding, J. Phys. Sci. E, Instrum. 3 (1970) 572;
(b) H.B. Tinker, D.E. Morris, Rev. Sci. Instrum. 7 (1972) 1024;
(c) W.E. Walker, L.A. Cosby, S.T. Martin, US Patent 38863641975, Union Carbide Corp.
[11] K. Noack, Spectrochim. Acta 24A (1917).
[12] R.B. King, A.D. King Jr., M.Z. Iqbal, C.C. Frazier, J. Am. Chem. Soc. 100 (1978) 1687.
[13] (a) W.R. Moser, J.E. Cnossen, A.W. Wang, S.A. Krouse, J. Catal. 95 (1985) 21;
(b) W.R. Moser, C.J. Papile, D.A. Brannon, R.A. Duwell, J. Mol. Catal. 41 (1987) 271.
[14] D. Evans, G. Yagupsky, G.J. Wilkinson, Chem. Soc. A (1968) 2660.
[15] (a) M. Garland, P. Pino, Organometallics 10 (1991) 1693;
(b) J. Feng, M. Garland, Organometallics 18 (1999) 417.
[16] A. Van Rooy, E. Orij, P.C.J. Kamer, P.W.N.M. Van Leeuwen, Organometallics 14 (1995) 34.
[17] T. Jongsma, G. Challa, P.W.N.M. Van Leeuwen, J. Organomet. Chem. 421 (1991) 121.

[18] More detailed information will be published separately. The described cell can be purchased from Ideas!UvA bv, Amsterdam, The Netherlands, 2004, price Euro 48,000.
[19] S.C. van der Slot, P.C.J. Kamer, P.W.N.M. van Leeuwen, J. Fraanje, K. Goubitz, M. Lutz, A.L. Spek, Organometallics 19 (2000) 2504.
[20] S.C. van der Slot, P.C.J. Kamer, P.W.N.M. van Leeuwen, J.A. Iggo, B.T. Heaton, Organometallics 20 (2001) 430.
[21] C.J. Elsevier, J. Mol. Catal. 92 (1994) 285.
[22] C.P. Casey, G.T. Whiteker, Isr. J. Chem. 30 (1990) 299.
[23] C.P. Casey, G.T. Whiteker, M.G. Melville, L.M. Petrovich, J.A. Gavney Jr., D.R. Powell, J. Am. Chem. Soc. 114 (1992) 5535.
[24] M. Kranenburg, Y.E.M. van der Burgt, P.C.J. Kamer, P.W.N.M. van Leeuwen, Organometallics 14 (1995) 3081.
[25] L.A. van der Veen, P.H. Keeven, G.C. Schoemaker, J.N.H. Reek, P.C.J. Kamer, P.W.N.M. van Leeuwen, M. Lutz, A.L. Spek, Organometallics 19 (2000) 872.
[26] L.A. van der Veen, P.C.J. Kamer, P.W.N.M. van Leeuwen, Angew. Chem. Int. Ed. 38 (1999) 336.
[27] L.A. van der Veen, P.C.J. Kamer, P.W.N.M. van Leeuwen, Organometallics 18 (1999) 4765.
[28] S.C. van der Slot, J. Duran, J. Luten, P.C.J. Kamer, P.W.N.M. van Leeuwen, Organometallics 21 (2002) 3873.
[29] P.W.N.M. van Leeuwen, Appl. Catal. A 212 (2001) 61.
[30] (a) P.W.N.M. van Leeuwen, C.F. Roobeek, J. Mol. Catal. 31 (1985) 345;
(b) A. van Rooy, J.N.H. de Bruijn, C.F. Roobeek, P.C.J. Kamer, P.W.N.M. van Leeuwen, J. Organomet. Chem. 507 (1996) 69.
[31] K.F. Muilwijk, P.C.J. Kamer, P.W.N.M. van Leeuwen, J. Am. Oil Chem. Soc. 74 (1997) 223.
[32] E. Billig, A.G. Abatjoglou, D.R. Bryant, R.E. Murray, J.M. Maher (to Union Carbide Corporation) US Patent 4,717,775, 1988, Chem. Abstr. 109 (1989) 233177.
[33] E. Walczuk, P.C.J. Kamer, P.W.N.M. van Leeuwen, Angew. Chem. Int. Ed. 42 (2003) 4665.
[34] (a) W.M. Ress, J.D. Atwood, Organometallics 4 (1985) 402;
(b) W.M. Ress, M.R. Churchil, Y.-J. Li, J.D. Atwood, Organometallics 4 (1985) 1162;
(c) W.M. Ress, M.R. Churchil, J.C. Fettinger, J.D. Atwood, Organometallics 4 (1985) 2179;
(d) M.R. Churchil, J.C. Fettinger, W.M. Ress, J.D. Atwood, J. Organomet. Chem. 304 (1986) 227.
[35] C. Crause, L. Bennie, L. Damoense, C.L. Dwyer, C. Grove, N. Grimmer, W.J. van Rensburg, M.M. Kirk, K.M. Mokheseng, S. Otto, P.J. Steynberg, Dalton Trans. (2003) 2036.